Skeletal Muscle–Specific Deletion of Lipoprotein Lipase Enhances Insulin Signaling in Skeletal Muscle but Causes Insulin Resistance in Liver and Other Tissues

Hong Wang,[1] Leslie A. Knaub,[1] Dalan R. Jensen,[1] Dae Young Jung,[2] Eun-Gyoung Hong,[2] Hwi-Jin Ko,[2] Alison M. Coates,[1] Ira J. Goldberg,[3] Becky A. de la Houssaye,[4] Rachel C. Janssen,[4] Carrie E. McCurdy,[4] Shaikh M. Rahman,[4] Cheol Soo Choi,[5] Gerald I. Shulman,[6] Jason K. Kim,[2] Jacob E. Friedman,[4] and Robert H. Eckel[1]

OBJECTIVE—Skeletal muscle–specific LPL knockout mouse ($SMLPL^{-/-}$) were created to study the systemic impact of reduced lipoprotein lipid delivery in skeletal muscle on insulin sensitivity, body weight, and composition.

RESEARCH DESIGN AND METHODS—Tissue-specific insulin sensitivity was assessed using a hyperinsulinemic-euglycemic clamp and 2-deoxyglucose uptake. Gene expression and insulin-signaling molecules were compared in skeletal muscle and liver of $SMLPL^{-/-}$ and control mice.

RESULTS—Nine-week-old $SMLPL^{-/-}$ mice showed no differences in body weight, fat mass, or whole-body insulin sensitivity, but older $SMLPL^{-/-}$ mice had greater weight gain and whole-body insulin resistance. High-fat diet feeding accelerated the development of obesity. In young $SMLPL^{-/-}$ mice, insulin-stimulated glucose uptake was increased 58% in the skeletal muscle, but was reduced in white adipose tissue (WAT) and heart. Insulin action was also diminished in liver: 40% suppression of hepatic glucose production in $SMLPL^{-/-}$ vs. 90% in control mice. Skeletal muscle triglyceride was 38% lower, and insulin-stimulated phosphorylated Akt (Ser473) was twofold greater in $SMLPL^{-/-}$ mice without changes in IRS-1 tyrosine phosphorylation and phosphatidylinositol 3-kinase activity. Hepatic triglyceride and liver X receptor, carbohydrate response element–binding protein, and PEPCK mRNAs were unaffected in $SMLPL^{-/-}$ mice, but peroxisome proliferator–activated receptor (PPAR)-γ coactivator-1α and interleukin-1β mRNAs were higher, and stearoyl–coenzyme A desaturase-1 and PPARγ mRNAs were reduced.

CONCLUSIONS—LPL deletion in skeletal muscle reduces lipid storage and increases insulin signaling in skeletal muscle without changes in body composition. Moreover, lack of LPL in skeletal muscle results in insulin resistance in other key metabolic tissues and ultimately leads to obesity and systemic insulin resistance. ***Diabetes*** **58:116–124, 2009**

From the [1]Division of Endocrinology, Metabolism and Diabetes, University of Colorado Denver Anschutz Medical Campus, Aurora, Colorado; the [2]Department of Cellular & Molecular Physiology, Pennsylvania State University College of Medicine, Hershey, Pennsylvania; the [3]Department of Medicine, Columbia University, New York City, New York; the [4]Department of Pediatrics, University of Colorado Denver Anschutz Medical Campus, Aurora, Colorado; the [5]Department of Internal Medicine, Yale University School of Medicine, New Haven, Connecticut; and the [6]Department of Internal Medicine, Department of Cellular & Molecular Physiology, Howard Hughes Medical Institute, Yale University School of Medicine, New Haven, Connecticut.

Corresponding author: Robert H. Eckel, robert.eckel@uchsc.edu.

Received 29 December 2007 and accepted 8 October 2008.

Published ahead of print at http://diabetes.diabetesjournals.org on 24 October 2008. DOI: 10.2337/db07-1839.

See accompanying commentary, p. 16.

Lipoprotein lipase (LPL) (European Commission no. 3.1.1.34) is a key enzyme in lipid metabolism and is described as a "gatekeeper" for its role in partitioning lipoprotein-derived free fatty acids (FFAs) between tissues (1). Once hydrolyzed, the lipoprotein-derived FFAs are available for uptake and use by extrahepatic tissues for either storage or oxidation. LPL is most abundant in heart, adipose tissue, and skeletal muscle (2,3). The importance of LPL in fuel partitioning and utilization is underscored by observations that tissue-specific perturbations in LPL activity result in dramatic shifts in body composition and lipid and glucose metabolism (4), particularly in heart and skeletal muscle.

We and others previously showed that mice with muscle-specific lipoprotein lipase overexpression are insulin resistant (5,6). Insulin resistance developed selectively in muscle, while insulin sensitivity in the liver was not affected. Overexpression of LPL in the skeletal muscle also led to excessive intramyocellular lipid deposition, suggestive of the relationship between lipid storage and insulin sensitivity.

To further investigate the systemic impact of skeletal muscle LPL (SMLPL) on lipoprotein-derived fatty acid partitioning between tissues and insulin sensitivity, we generated skeletal muscle–specific LPL knockout mice, denoted $SMLPL^{-/-}$. We hypothesized that SMLPL is an important interface through which lipid-derived signals are integrated to regulate insulin signaling and that SMLPL deletion would perturb the balance of fuel utilization not only in skeletal muscle but also in other insulin-sensitive tissues.

RESEARCH DESIGN AND METHODS

Animals. Studies were conducted in accordance to protocols approved by institutional animal care and use committees (University of Colorado Denver Anschutz Medical Campus, Pennsylvania State University). $SMLPL^{-/-}$ mice were generated by the *cre*-lox system. Transgenic mice with floxed LPL (7) were crossed with transgenic mice in which skeletal muscle–specific expression of *cre* recombinase was driven by the myosin light chain 1f gene promoter (8). Offspring were then crossed with each other to produce mice with at least one *cre* allele and either two floxed LPL alleles or two wild-type LPL alleles. The presence of the *cre* transgene and either wild-type or floxed LPL was verified by PCR.

Male 9- to 11-week-old (young) or 8- to 10-month-old (old) $SMLPL^{-/-}$ and wild-type littermate control mice were housed at ~20°C on a 12:12 h light:dark photoperiod and provided standard rodent food and water ad libitum. For high-fat (HF) diet feeding, 6-week-old $SMLPL^{-/-}$ and control mice were put on an HF diet (Research Diet, 45% fat) and a 10% low-fat (LF) diet matched for other nutrient content for 6 weeks. Unless specified, mice were anesthe-

tized with intraperitoneal administration of Avertin (250 mg/kg 2,2,2-tribromoethanol) after a 4-h fast.

Glucose and insulin tolerance tests. Glucose and insulin tolerance tests were performed by bolus intraperitoneal injection of glucose (1 g/kg) or insulin (0.75 units/kg), respectively. Blood glucose was measured from the tail using a glucometer (OneTouch Ultra, Lifescan) at baseline (0) and 10, 20, 30, 45, 60, and 90 min after injection.

LPL activity assay. Tissues were dissected and assayed immediately. Heparin-releasable LPL activity was measured in heart, white adipose tissue (WAT), red skeletal muscle (soleus and red gastrocnemius), and white skeletal muscle (white gastrocnemius) as previously described (9). LPL activity was expressed as nanomoles of FFA per minute per gram of tissue.

Measurement of body composition, plasma profiles, and tissue lipid content. Body composition was measured on anesthetized mice by dual-energy X-ray absorptiometry using a mouse densitometer (PIXImus2; Lunar, Madison, WI). Blood was collected by cardiac puncture, and plasma was stored at −80°C until further analysis. Plasma glucose was measured using the Analox GM7 (Analox Instruments, Lunenburg, MA), FFAs were measured using enzymatic colorimetric assays (Wako Chemicals, Richmond, VA), and insulin was measured using a radioimmunoassay kit (Linco Research, St. Charles, MO). Plasma cholesterol was measured on an Olympus AU400e chemistry analyzer (Olympus America, Center Valley, PA). Plasma leptin, adiponectin, interleukin (IL)-1β, and IL-6 were measured using specific enzyme-linked immunoassay (ELISA) kits (Alpco Diagnostics, Salem, NH). Red skeletal muscle, liver, and heart tissue were excised, flash-frozen, and stored at −80°C until triglyceride (TG) content was measured as previously described (10). Long-chain fatty acyl–coenzyme A (LC acyl-CoA) was extracted and purified from skeletal muscle using methods described previously (11,12). After purification, LC acyl-CoA fractions were dissolved in methanol/H_2O (1:1; vol/vol) and subjected to liquid chromatography/tandem MS analysis (13). Diacylglycerol (DAG) and ceramide extraction and analysis were performed as described previously (13,14). Total LC acyl-CoA, DAG, and ceramides are expressed as the sum of individual species.

Indirect calorimetry measurements. An open-ended indirect calorimetry system was used to measure oxygen consumption O_2 and CO_2 production in mice for the calculation of metabolic rate and respiratory quotient (15). Animals were placed in metabolic chambers for measurements taken over at least 2 days with free access to food and water.

Hyperinsulinemic-euglycemic clamps. This study was performed at the Penn State Mouse Metabolic Phenotyping Center, and the procedures were approved by the Pennsylvania State University Institutional Animal Care and Use Committee. At 4–5 days before clamp experiments, mice were anesthetized, and an indwelling catheter was inserted in the right internal jugular vein (16). On the day of the clamp experiment, a three-way connector was attached to the catheter to intravenously deliver solutions. After an overnight fast (~15 h), a 2-h hyperinsulinemic-euglycemic clamp was conducted in awake SMLPL$^{-/-}$ mice and wild-type littermates with a primed (150 mU/kg body wt) and continuous infusion of insulin (Humulin; Eli Lilly, Indianapolis, IN) at a rate of 2.5 mU · kg^{-1} · min^{-1} to raise plasma insulin within a physiological range. Blood samples (20 μl) were collected at 20-min intervals for measurement of plasma glucose concentration, and 20% glucose was infused at variable rates to maintain glucose at basal concentrations. Basal and insulin-stimulated whole-body glucose turnover were estimated with a continuous infusion of [3-^{3}H]glucose (PerkinElmer, Boston, MA) for 2 h before the clamps (0.05 μCi/min) and throughout the clamps (0.1 μCi/min), respectively. To estimate insulin-stimulated glucose uptake in individual organs, 2-deoxy-D-[1-^{14}C]glucose (2-[^{14}C]-DG) was administered as a bolus (10 μCi) at 75 min after the start of clamps. At the end of the clamps, mice were anesthetized, and tissues were taken for biochemical analysis.

In vitro 2-deoxyglucose uptake in muscle. To measure 2-deoxyglucose (2-DG) uptake, paired soleus were dissected from anesthetized mice and incubated at 37°C for 30 min in oxygenated (95% O_2, 5% CO_2) flasks of Krebs-Henseleit buffer (KHB) containing the following, with or without 50 μU/ml insulin: 0.1% BSA, 2 mmol/l Na-pyruvate, and 6 mmol/l mannitol. After 30 min, muscles were transferred to a second flask and incubated at 37°C for 20 min in KHB plus 0.1% BSA, 9 mmol/l [^{14}C]-mannitol, and 1 mmol/l [^{3}H]-2-DG (0.053 and 3 mCi/mmol, respectively; Perkin Elmer, Boston, MA) with the same insulin concentration. After 20 min, muscles were blotted on ice-cold filter paper, trimmed, and freeze-clamped and then stored (−80°C). Frozen muscles were weighed and homogenized as previously described (17). The homogenate was transferred to microfuge tubes and solubilized (1–2 h, 4°C) with end-over-end rotation. The homogenate was centrifuged (12,000*g*, 12 min, 4°C) and used immediately for 2-DG uptake measurement. 2-DG uptake rate was calculated as previously described (18).

Insulin signaling. Basal and insulin-stimulated red skeletal muscle, WAT, and insulin-stimulated liver were collected from young anesthetized mice as described previously (10). After a 10 units/kg dose of insulin (Humulin), administered via the inferior vena cava, tissues were flash-frozen in liquid nitrogen and stored at −80°C until analysis. Basal liver tissues were collected from a different set of mice that did not receive insulin.

For Western blot analysis, tissues were homogenized in cell lysis buffer (10). A total of 50 μg protein was electrophoresed on 8% or 10% precast SDS-PAGE gels and transferred onto a PVDF membrane. Blots were probed with antibodies for IR and IRS-1 phospho-tyrosine (P-Tyr-100), phospho-Akt (S473), and phosphor-Akt (T308) (all from Cell Signaling) first and then stripped and probed again with antibodies for total IR (Santa Cruz), IRS-1 (Upstate), Akt, PTEN, and SHIP2 (Cell Signaling). Results were detected by chemiluminescence (ECL; Amersham Biosciences, Piscataway, NJ) and visualized on X-ray films and analyzed using an HC Precision Scan Pro and Bio-Rad Quantity One Analysis Software. An internal standard (wild-type mouse homogenate) was used to normalize results and to control for blot-to-blot variation.

The level of IRS-1–associated PI 3-kinase activity was determined in muscle extracts after immunoprecipitation with IRS-1 antibody/agarose conjugate overnight at 4°C (19).

Quantitative real-time PCR. Red skeletal muscle, white skeletal muscle, liver, WAT, and heart were collected from young anesthetized mice, flash-frozen, and stored at −80°C until processing. Total RNA was extracted from homogenized tissue using both TRIZOL reagent (Invitrogen) and RNeasy Mini Kit (Qiagen). One-step RT-PCR was performed using 50 ng total RNA with iScript One-Step RT-PCR Kit for Probes (Bio-Rad, Hercules, CA) and TaqMan Gene Expression Assays (ABI, Foster City, CA). For three internal reference genes, one-step RT-PCR was performed using an iScript One-Step RT-PCR Kit with SYBR Green (Bio-Rad). Reactions were run in duplicate on an iQ5 Real-Time PCR Detection System (Bio-Rad) along with no-template controls per gene. The cycling conditions comprised 10-min cDNA synthesis at 50°C, 5-min reverse transcriptase inactivation at 95°C, and 45 cycles at 95°C for 10 s and 60°C for 30 s. RNA expression data were normalized to levels of ubiquitin C (Ubc) RNA, hypoxanthine guanine phosphoribosyl transferase 1 (Hprt1) RNA, and actin beta (Actb) RNA using the comparative threshold cycle method. Ubc, Hprt1, and Actb primer sets, as described in the study by Vandesompele et al. (18a), were as follows: Ubc forward primer 5′-AGGTCAAACAGGAAGACAGACGTA-3′, Ubc reverse primer 5′-TCACACCCAAGAACAAGCACA-3′; Hprt1 forward primer 5′-AGTGTTGGATACAGGCCAGAC-3′, Hprt1 reverse primer 5′-CGTGATTCAAATCCCTGAAGT-3′; and Actb forward primer 5′-ATGCTCCCCGGGCTGTAT-3′, Actb reverse primer 5′-CATAGGAGTCCTTCTGACCCATTC-3′.

Statistical analysis. Results are presented as means ± SE. The *t* tests were performed using SigmaStat 2.03 (San Rafel, CA). $P < 0.05$ was considered significant.

RESULTS

Skeletal muscle–specific LPL ablation (SMLPL$^{-/-}$). In 9- to 11-week-old SMLPL$^{-/-}$ mice, RT-PCR showed a 83% reduction ($P < 0.001$) in LPL mRNA expression in the red skeletal muscle, with only 50% reduction in white skeletal muscle and no change in the heart (Fig. 1*A*). Skeletal muscle LPL activity was decreased by 72% ($P < 0.001$) in the predominantly red muscle fibers of the soleus and red gastrocnemius muscles (Fig. 1*B*). White muscle LPL activity was 22% lower in SMLPL$^{-/-}$ mice and was not statistically significant ($P = 0.131$). LPL activities in heart and WAT were not affected.

Body composition, plasma metabolite profiles, and energy balance. The reduction of LPL activity in skeletal muscle did not alter body composition of 9- to 11-week-old SMLPL$^{-/-}$ mice (Fig. 1*C*, *left panel*; Table 1). However, at 8–10 months of age, SMLPL$^{-/-}$ mice were heavier than controls with most of the extra weight fat mass (Fig. 1*C*, *right panel*).

Whole-body metabolic rate, respiratory quotient, and energy intake were also not different between the two groups of young mice (Table 1). After a 4-h fast, plasma glucose, insulin, total and lipoprotein cholesterol, and FFA levels were similar between young SMLPL$^{-/-}$ and control mice, with a trend for higher TGs ($P = 0.074$) in SMLPL$^{-/-}$ mice (Table 2). Plasma leptin, adiponectin, IL-1β, and IL-6

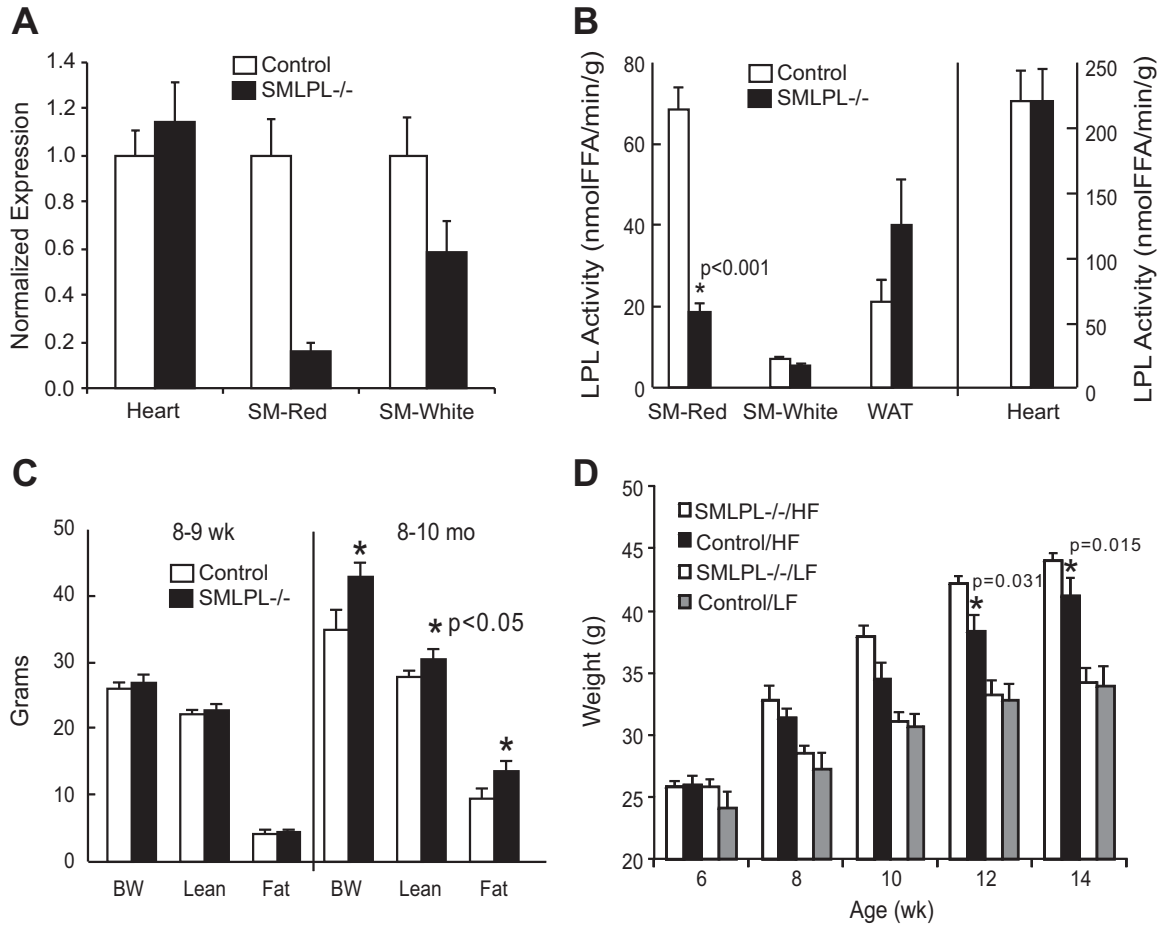

FIG. 1. *A*: **mRNA expression of LPL in muscle tissues. LPL mRNA expression was measured in red skeletal muscle (SM-Red), white skeletal muscle (SM-White), and heart using RT-PCR. $n = 3$ for both SMLPL$^{-/-}$ and control mice.** *B*: **Tissue-specific LPL activities in young SMLPL$^{-/-}$ mice. Heparin-releasable LPL activities were measured for skeletal red muscle (SM-Red), skeletal white muscle (SM-White), WAT, and heart from both the 9- to 11-week-old SMLPL$^{-/-}$ and control mice. LPL activities were expressed as nanomoles of FFA per minute per gram of tissue. $n = 8$ for SMLPL$^{-/-}$ and $n = 10$ for control mice.** *C*: **Weight, lean mass, and fat mass comparisons between young and old SMLPL$^{-/-}$ mice. The body weights of young (8–9 weeks) and old (8–10 months) SMLPL$^{-/-}$ mice were compared. Body compositions were determined by dual-energy X-ray absorptiometry. $n = 5$ for both SMLPL$^{-/-}$ and control mice at different ages.** *D*: **Weight gain in HF-fed SMLPL$^{-/-}$ mice. The body weights of 6-week-old SMLPL$^{-/-}$ and control mice that are subjected to either HF or LF diet were monitored every 2 weeks for 6 weeks. $n = 6$ for each group of mice.**

also were not different between the two groups at 9–11 weeks of age (Table 2).

To determine whether high-fat feeding might accelerate the obesity phenotype, 6-week-old SMLPL$^{-/-}$ mice were subjected to the HF diet for 6 weeks (Fig. 1*D*). After 4 weeks on the HF diet, SMLPL$^{-/-}$ mice were heavier than control mice ($P = 0.031$ for 4 weeks; $P = 0.015$ for 6 weeks).

TABLE 1
General characterization of 9- to 11-week-old SMLPL$^{-/-}$ and control mice

	Control	SMLPL$^{-/-}$
Body weight (g)	26.87 ± 0.69	27.00 ± 0.80
Lean mass (g)	22.1 ± 0.5	22.2 ± 0.7
Fat mass (g)	3.8 ± 0.3	3.8 ± 0.3
Percent fat	14.6 ± 0.7	14.5 ± 0.7
Energy intake (kcal/day)	13.43 ± 1.68	11.92 ± 1.59
MR (kcal · day^{-1} · g^{-1} lean body mass × 0.75)	1.80 ± 0.07	1.76 ± 0.09
Respiratory quotient	0.89 ± 0.02	0.92 ± 0.02

$n = 8$ for both groups of mice. MR, metabolic rate.

Glucose tolerance and insulin tolerance tests. Although blood glucose, insulin, and insulin tolerance were not altered in chow-fed young mice (Fig. 2*A* and *B*), SMLPL$^{-/-}$ mice developed glucose intolerance by 6 months of age (Fig. 2*C*). Moreover, HF-fed SMLPL$^{-/-}$ mice

TABLE 2
Plasma lipids, metabolites, and cytokines in 9- to 11-week-old SMLPL$^{-/-}$ and control mice

	Control	SMLPL$^{-/-}$
Glucose (mmol)	10.0 ± 1.2	9.5 ± 1.2
Insulin (ng/ml)	0.66 ± 0.30	0.45 ± 0.30
FFA (mmol/l)	0.58 ± 0.10	0.66 ± 0.11
Total cholesterol (mg/dl)	102 ± 15	128 ± 33
HDL cholesterol (mg/dl)	56 ± 8	61 ± 13
LDL cholesterol (mg/dl)	31 ± 6	24 ± 7
Triglycerides (mg/dl)	77 ± 45	219 ± 92
Leptin (ng/ml)	1.3 ± 1.6	3.1 ± 2.5
Adiponectin (mg/ml)	33 ± 14	33 ± 5
IL-1β (pg/ml)	28 ± 19	20 ± 11
IL-6 (pg/ml)	32 ± 27	15 ± 2

$n = 8$ for glucose, insulin, and FFA measurement for both groups of mice. $n = 6$ for all other measurements.

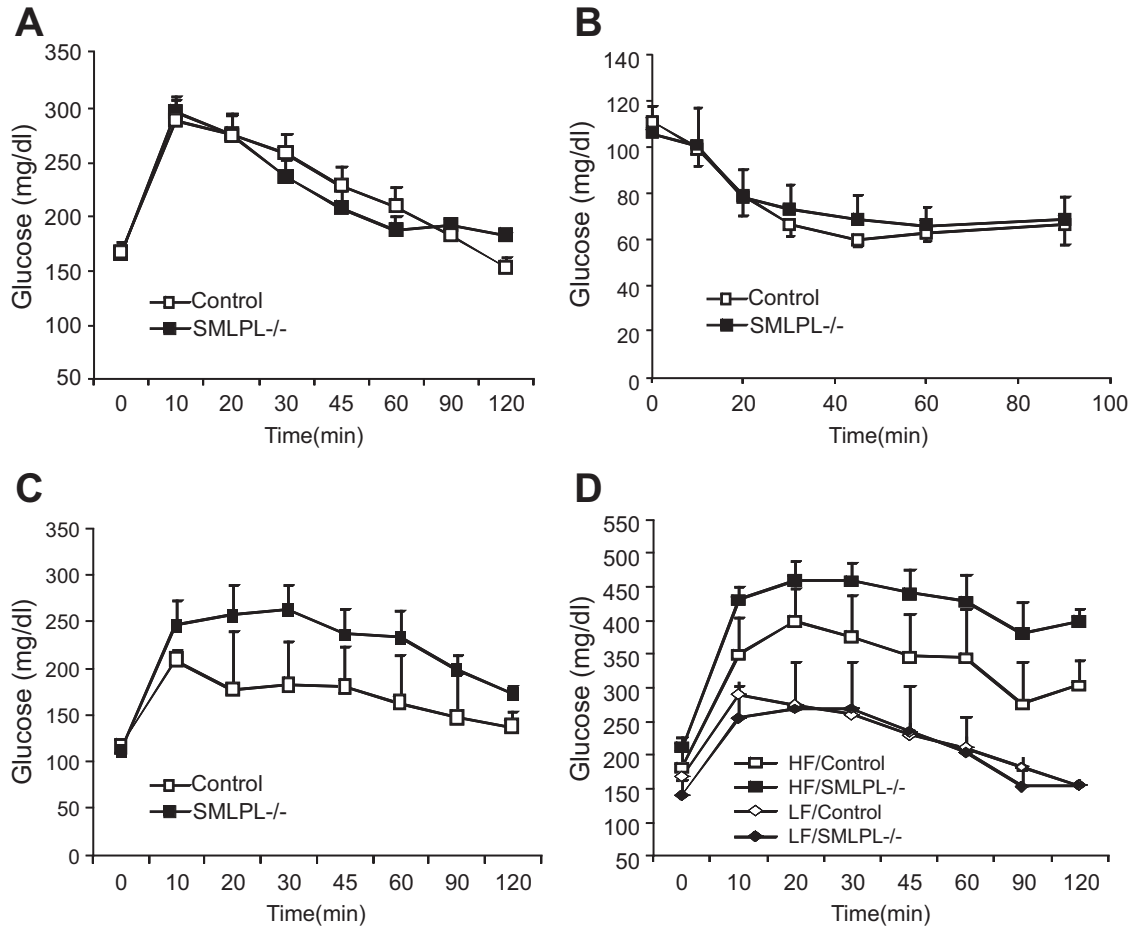

FIG. 2. Glucose tolerance test and insulin tolerance test of SMLPL$^{-/-}$ mice. Time courses of blood glucose levels in young SMLPL$^{-/-}$ and control mice after intraperitoneal injection of 1 g/kg glucose (*A*) or 0.75 units/kg insulin (*B*) are shown. Time courses are also shown of blood glucose levels in 6-month-old SMLPL$^{-/-}$ and control mice after intraperitoneal injection of 1 g/kg glucose (*C*) and for 12-week-old SMLPL$^{-/-}$ and control mice that have been subjected to different diet for 6 weeks (*D*). $n = 6$ for the glucose tolerance test, and $n = 5$ for SMLPL$^{-/-}$; $n = 4$ for control mice in the insulin tolerance test.

had elevated plasma glucose levels compared with HF-fed control mice (Fig. 2*D*).

Whole-body insulin sensitivity and tissue-specific glucose metabolism. Insulin sensitivity in 9- to 11-week-old mice was comparable between SMLPL$^{-/-}$ and control mice with glucose infusion rates of 39 ± 4 and 44 ± 4 mg · kg^{-1} · min^{-1}, respectively (Fig. 3*A*, *left*). Of great interest, however, SMLPL$^{-/-}$ mice displayed a reduced capacity of insulin to suppress hepatic glucose production with only 39 ± 8% suppression (from 19.1 to 11.1 mg · kg^{-1} · min^{-1}) compared to 91 ± 8% suppression (from 20.5 to 0.4 mg · kg^{-1} · min^{-1}) in the control mice ($P = 0.001$) (Fig. 3*A*, *right*). At 8–10 months, SMLPL$^{-/-}$ mice developed systemic insulin resistance (Fig. 3*B*).

More surprisingly, 2-DG uptake measured at the end of the clamp was increased in skeletal muscle of the young SMLPL$^{-/-}$ mice (539 ± 48 vs. 341 ± 20 nmol · g^{-1} · min^{-1}, $P = 0.003$) but was greatly reduced in WAT (11 ± 3 vs. 51 ± 9 nmol · g^{-1} · min^{-1}, $P = 0.003$) and heart (1,798 ± 359 vs. 3,257 ± 223 nmol · g^{-1} · min^{-1}, $P = 0.006$) (Fig. 3*C*). A trend for reduced glucose uptake was also observed in brown adipose tissue of SMLPL$^{-/-}$ mice (582 ± 90 vs. 1,552 ± 424 nmol · g^{-1} · min^{-1}, $P = 0.072$).

The maximal glucose transport activity in isolated soleus muscle was measured for both young SMLPL$^{-/-}$ and control mice (Fig. 3*D*). In control mice, glucose transport was increased 40% upon insulin stimulation. In SMLPL$^{-/-}$ mice, basal glucose transport was increased 25% compared with control mice, and it was further increased 80% upon insulin stimulation ($P = 0.01$ vs. control). Thus, skeletal muscle from young SMLPL$^{-/-}$ mice displayed a higher basal glucose transport activity and was more responsive to insulin both in vivo and ex vivo.

These findings indicated that skeletal muscle–specific deletion of LPL in young mice increased insulin sensitivity selectively in skeletal muscle but caused insulin resistance in liver, heart, and adipose tissues, suggesting that reciprocal changes in insulin action in different tissues might be responsible for the lack of changes in whole-body insulin sensitivity.

Skeletal muscle TG content reduced with no change in other lipid metabolites. To understand whether changes in cellular and circulating lipids might underlie the changes in insulin sensitivity in SMLPL$^{-/-}$ mice, we measured TG content in skeletal muscle, liver, and heart (Fig. 4*A*). SMLPL$^{-/-}$ mice showed a 40% reduction ($P = 0.045$) in skeletal muscle TG, with no difference in liver TG. Yet there were no differences in intramuscular total LC acyl-CoA, total DAG, or total ceramide levels in SMLPL$^{-/-}$ and control mice (Fig. 4*B*). Heart TG was not different ($P = 0.126$) in SMLPL$^{-/-}$ mice (Fig. 4*A*).

Increased insulin signaling in skeletal muscle. Because glucose uptake in the skeletal muscle was higher in the SMLPL$^{-/-}$ mice during the hyperinsulinemic clamp,

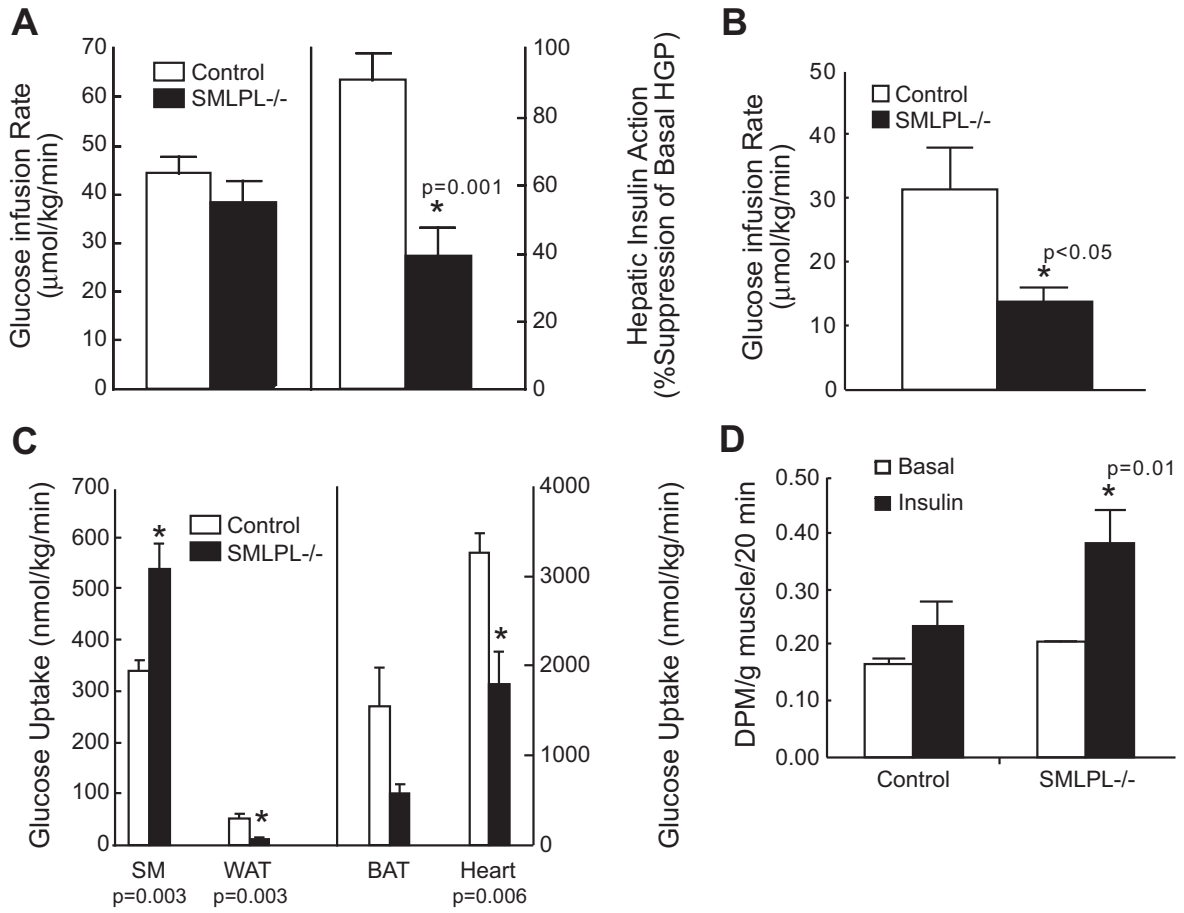

FIG. 3. Whole-body insulin sensitivity and tissue-specific glucose uptake in vivo in the SMLPL$^{-/-}$ and control mice. *A*: Steady-state whole-body glucose infusion rate during hyperinsulinemic-euglycemic clamps and hepatic insulin action as the percent suppression of basal hepatic glucose production during the clamps for young SMLPL$^{-/-}$ mice. $n = 5$ for both SMLPL$^{-/-}$ and control mice. *B*: Steady-state whole-body glucose infusion rate during hyperinsulinemic-euglycemic clamps for old SMLPL$^{-/-}$ mice. $n = 5$ for both SMLPL$^{-/-}$ and control mice. *C*: Tissue-specific glucose uptake. Insulin-stimulated glucose uptake in skeletal muscle (gastrocnemius, SM), WAT, brown adipose tissue (BAT), and heart were measured by injecting a bolus of 2-[^{14}C]-DG during the clamp. $n = 5$ for SMLPL$^{-/-}$ and $n = 6$ for control mice. *D*: Insulin-stimulated glucose transport in soleus muscle of SMLPL$^{-/-}$ mice ($n = 3$ for both SMLPL$^{-/-}$ and control mice). DPM, disintegrations per minute.

we investigated whether this was due to changes in the insulin-signaling cascade. Surprisingly, there were no differences in the total levels of IR, IRS-1, Akt, insulin-stimulated tyrosine phosphorylation of the insulin receptor or IRS-1, or PI 3-kinase activation (Fig. 5*A–C*). However, we observed a nearly twofold increase in net insulin-stimulated Ser473 Akt activation ($P < 0.01$) upon insulin stimulation (Fig. 5*D*) in the red muscle of the SMLPL$^{-/-}$ mice. Full activation of Akt also requires the phosphorylation of threonine 308 of the activation loop in Akt by PDK1 (20). SMLPL$^{-/-}$ mice showed a 40% increase in Thr308 Akt phosphorylation under basal conditions ($P = 0.05$), while insulin induced a similar 50% increase of Thr308 Akt phosphorylation in SMLPL$^{-/-}$ and control mice (Fig. 5*E*). The levels of two lipid phosphatases known to modify Akt phosphorylation (PTEN and SHIP2) (21,22) were unchanged in SMLPL$^{-/-}$ mice (Fig. 5*F*).

Examination of the insulin-signaling cascade in liver and WAT showed no differential activation (data not shown). Specifically, and unlike the response to insulin in red skeletal muscle, the level of insulin-stimulated Akt phosphorylation was not different in the liver or the WAT of the two groups of mice.

Gene regulation in skeletal muscle and liver. Quantitative real-time PCR (qRT-PCR) was performed to examine whether the loss of SMLPL affected important genes involved in lipid, glucose, and fatty acid metabolism in the skeletal red muscle (Fig. 6*A*). In eight representative genes examined, the mRNA expression levels of peroxisome proliferator–activated receptor (PPAR)α, PPARγ, tumor necrosis factor (TNF)-α, carnitine palmitoyl transferase-2, CD36, acetyl–coenzyme A carboxylase 2, and fibroblast growth factor 21 were not altered. Interestingly, the mRNA level of PPARγ coactivator (PGC)-1α was increased by 60% in the skeletal red muscle of SMLPL$^{-/-}$ mice ($P = 0.01$).

Similar qRT-PCR was performed on the liver of SMLPL$^{-/-}$ and control mice. A total of 13 representative genes were compared (Fig. 6*B*), and none of the gluconeogenic genes examined (PEPCK and glucose-6-phosphatase) showed differential expression. IL-1β expression was increased by 64% ($P = 0.034$), and PGC-1α expression was increased by 73% ($P = 0.005$) in SMLPL$^{-/-}$ liver. On the other hand, the hepatic gene expression levels for SCD-1 and PPARγ mRNA were significantly lower (69 and 57%, respectively) in SMLPL$^{-/-}$ mice ($P = 0.049$ and $P = 0.001$, respectively).

A comparison of 10 representative genes in WAT showed a trend for an increase in genes related to inflammatory pathways: CD68, IL-1β, IL-6, and TNF-α; however, these changes were not statistically significant (data not shown).

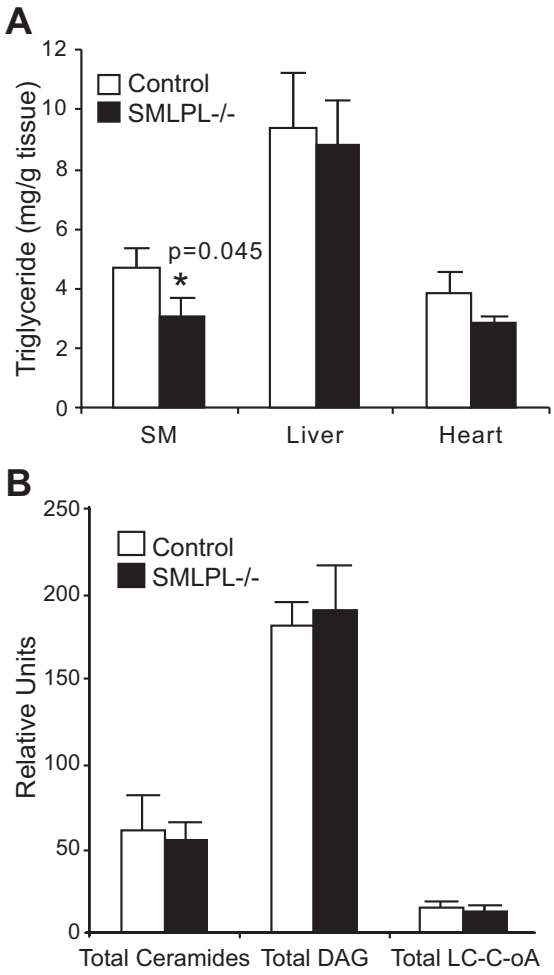

FIG. 4. Intracellular TG and lipid metabolite concentrations in skeletal muscle, liver, and heart. *A*: Intracellular TG concentrations in skeletal muscle, liver, and heart. $n = 8$ for SMLPL$^{-/-}$ and $n = 10$ for control mice for skeletal muscle, $n = 4$ for liver, and $n = 6$ for heart. *B*: Intracelluar LC acyl-CoA, DAG, and ceramides levels in skeletal muscle. $n = 8$ for both groups of mice.

DISCUSSION

Lipid partitioning between tissues is important to insulin action, energy balance, and the regulation of body weight and composition. The normal physiology of lipid and lipoprotein fuel partitioning is controlled by the transport and uptake of adipose tissue–derived FFA and lipoprotein-derived TG fatty acids. Tissue-specific changes in the regulation of LPL in obese subjects may play an important role in nutrient partitioning when energy intake exceeds energy expenditure (23–27). Thus, the ability to selectively modify LPL in skeletal muscle and/or adipose tissue may influence body weight and composition. The SMLPL$^{-/-}$ mice were created to provide a model to study how reduced lipid partitioning to skeletal muscle influences insulin-sensitive tissues and the potential role in regulating body weight, body composition, and whole-body insulin sensitivity.

SMLPL$^{-/-}$ mice show a transition of phenotypes between young and old animals. At a young (9–11 weeks) age, body weight and percent fat were unchanged compared with WT controls. With aging, both body weight and percent fat were increased in SMLPL$^{-/-}$ and systemic insulin resistance developed. The transition of the phenotype was accelerated by feeding the young SMLPL$^{-/-}$ mice with HF diets. Such information suggests an increased propensity that lipid storage develops and that accompanies lower lipid deposition in skeletal muscle.

The deletion of LPL in skeletal muscle results in two distinct patterns of clinical and biochemical abnormalities in young mice. The first is an increase in insulin sensitivity in skeletal muscle. The second is the decrease of insulin sensitivity in liver and other tissues. The present data suggest that skeletal muscle, and LPL in particular, acts as an important buffer against excess lipid storage but cannot protect against the ultimate development of obesity or insulin resistance. Despite no change in body composition in young SMLPL$^{-/-}$ mice or whole-body glucose disposal during the hyperinsulinemic clamp, closer inspection of individual tissues revealed that insulin-stimulated 2-DG uptake was significantly greater in skeletal muscle, whereas other insulin-sensitive tissues (WAT, heart) showed remarkable reductions in insulin-stimulated glucose uptake.

The increase in insulin-stimulated glucose uptake in skeletal muscle of young SMLPL$^{-/-}$ mice was associated with reduced TG accumulation in skeletal muscle and increased basal and insulin-stimulated Akt phosphorylation. Interestingly, there were no differences in the accumulation of other metabolic intermediates such as LC acyl-CoAs, ceramides, and DAG in skeletal muscle. Unexpectedly, the significant effect on increased Akt phosphorylation in SMLPL$^{-/-}$ mice was not associated with greater IRS-1 or PI 3-kinase activity. This suggests that LPL may play a role in regulating other lipid-derived factors that affect Akt phosphorylation in skeletal muscle.

Because the total PTEN and SHIP2 levels were not different in SMLPL$^{-/-}$ versus control mice, it is unlikely that these two negative regulators of Akt activity contribute to the increased Akt phosphorylation we observed in SMLPL$^{-/-}$ mice. Increased Akt phosphorylation at Ser473 has been associated with the mammalian target of rapamycin(mTOR)-rictor complex (28,29). Because there was no change in the Ser–IRS-1 phosphorylation (an mTOR target), it suggests that there may be other regulators of Akt in SMLPL$^{-/-}$ mice. For example, phosphorylation of Akt at Thr308 and Ser473 can be inhibited by direct binding of two different proteins: carboxyl-terminal modulator protein or TRB3 (30,31). Also, a pH domain leucine-rich repeat protein phosphatase (PHLPP) has also been shown to specifically dephosphorylate Ser-473 and inactivate Akt (32). Interestingly, insulin-stimulated Akt Thr308 phosphorylation was unaffected in SMLPL$^{-/-}$ mice, suggesting that there might be different combination of pathways affecting Akt activation. In subsequent studies, it will be important to identify which of these possible mediators might serve as the link between reduced LPL-mediated lipid uptake and deposition and enhanced Akt activation in our SMLPL$^{-/-}$ mice.

Increased insulin-stimulated glucose uptake and lower TG in skeletal muscle of young SMLPL$^{-/-}$ mice also suggest that the loss of LPL activity in skeletal muscle in SMLPL$^{-/-}$ mice creates a preference for glucose rather than TG-rich lipoproteins for fuel. Because plasma lipoprotein TG and liver TG were not statistically different for SMLPL$^{-/-}$ and control mice, more TG-rich lipoprotein TG may be processed in liver, WAT, or heart. Noting that LPL activity in WAT tissue was only marginally increased in SMLPL$^{-/-}$ mice and the fat mass remained the same as control mice, WAT tissue could be compensating for the loss of LPL in skeletal muscle by enhancing lipoprotein-dependent lipid uptake and turnover. However, at 9–11 weeks, there was no increase in TG storage in the heart, an

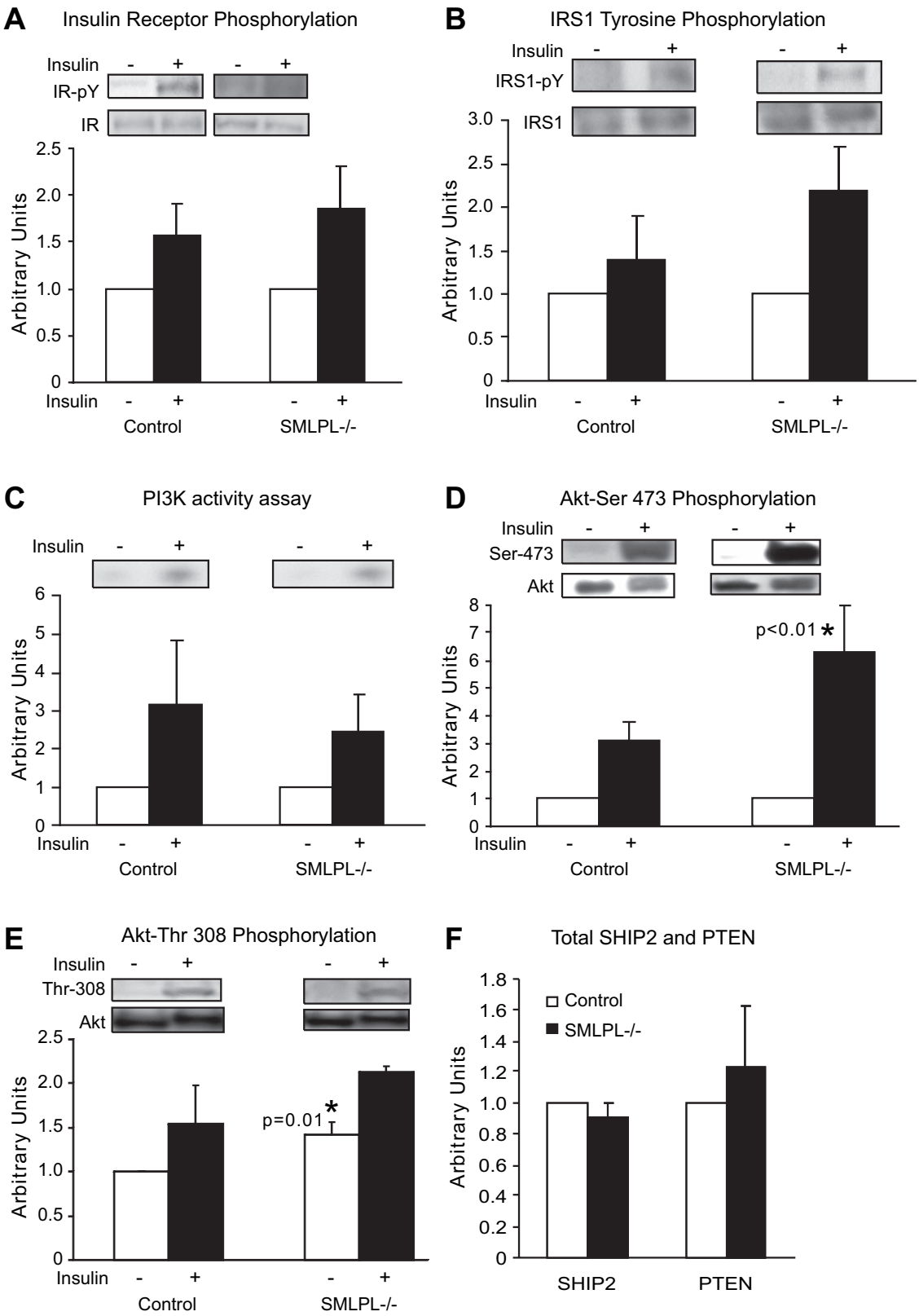

FIG. 5. Insulin signaling in red skeletal muscle of the SMLPL$^{-/-}$ mice. Tyrosine phosphorylation levels of insulin receptor (*A*) and IRS-1 (*B*), PI 3-kinase activity (*C*), Ser473 phosphorylation level of Akt (*D*), and Thr308 phosphorylation level of Akt (*E*) were compared for the red skeletal muscle of both SMLPL$^{-/-}$ and control mice before and after insulin stimulation. Total SHIP2 and PTEN (*F*) were compared for the red skeletal muscle of both SMLPL$^{-/-}$ and control mice at basal condition. For *A*, *B*, *D*, and *F*, $n = 4$ for control mice and $n = 5$ for SMLPL$^{-/-}$ mice. For *C* and *E*, $n = 3$ for control and SMLPL$^{-/-}$ mice.

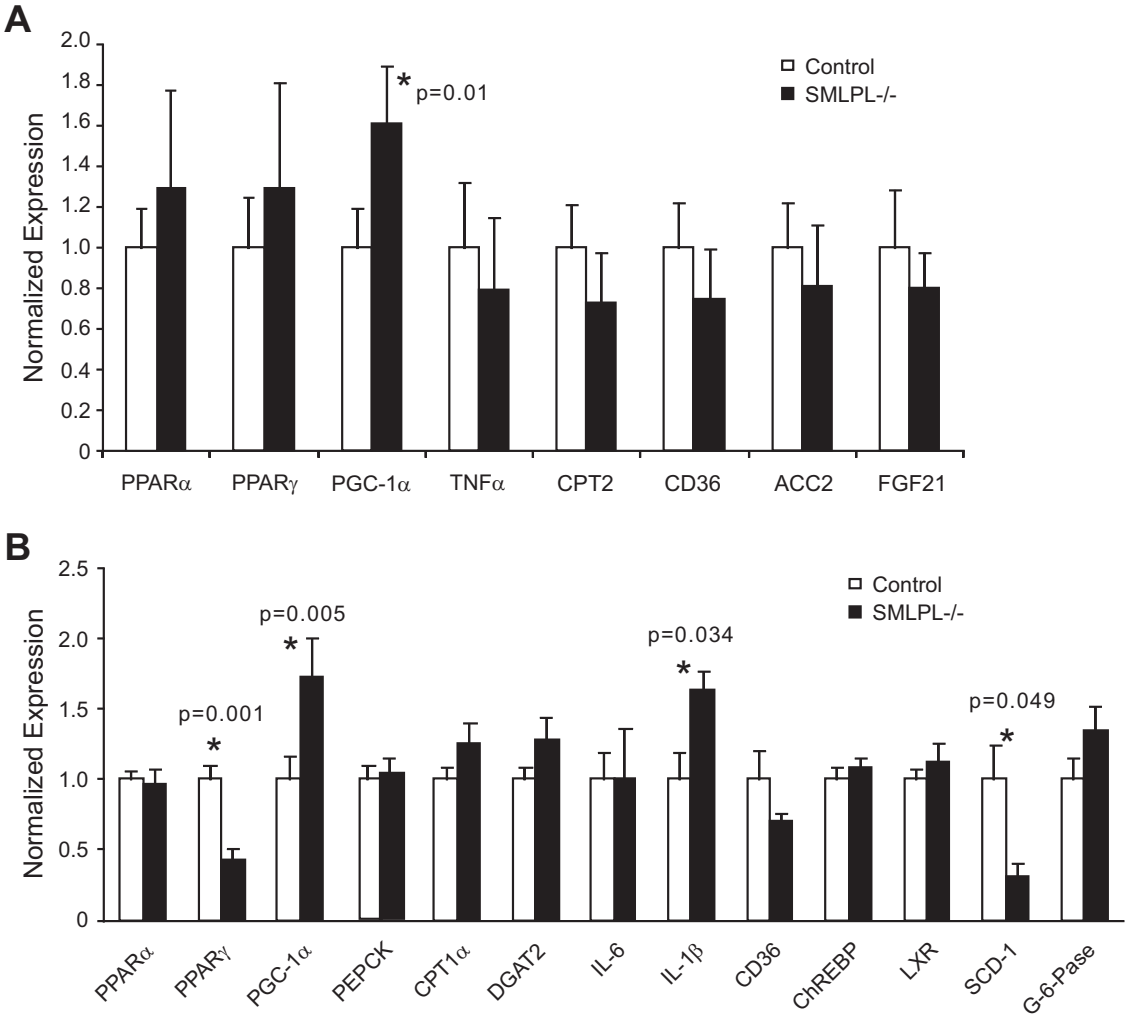

FIG. 6. Gene expression profiling in the skeletal muscle and liver of SMLPL mice. Expression levels of seven representative genes in red skeletal muscle were assessed by RT-PCR for both SMLPL$^{-/-}$ and control mice (*A*). *n* = 5 for both groups of mice. Expression levels of 13 representative genes in liver (*B*) of both the SMLPL$^{-/-}$ and control mice were assessed by RT-PCR. *n* = 6 for SMLPL$^{-/-}$ and *n* = 7 for control mice.

important organ in the metabolism of TG-rich lipoproteins. It is very likely at this stage of phenotypic development that the heart increased fatty acid oxidation in response to the reduced lipid partitioning to skeletal muscle.

Despite increased skeletal muscle insulin sensitivity, SMLPL$^{-/-}$ mice also displayed hepatic insulin resistance, as indicated by the reduced capacity to suppress hepatic glucose production upon insulin stimulation. However, TG content in the liver of SMLPL$^{-/-}$ mice was not increased. Gene expression in the liver of SMLPL$^{-/-}$ mice was mostly unchanged, whereas PGC-1α and IL-1β expression was modestly increased, and PPAR-γ and SCD-1 mRNA levels reduced in the liver of SMLPL$^{-/-}$ mice. The increase in IL-1β expression suggests a possible role of this cytokine in mediating insulin resistance in liver. However, when we measured the plasma IL-1β and IL-6 levels in SMLPL$^{-/-}$ mice, there was no indication that the circulating cytokine levels were elevated in the plasma of the mice.

The downregulation of PPAR-γ and SCD-1 in liver of the SMLPL$^{-/-}$ mice is consistent with the liver not storing excessive TG in the SMLPL$^{-/-}$ mice. SCD-1 catalyzes the desaturation of saturated fatty acyl-CoAs and is regulated by liver X receptor (LXR) (33). LXR gene expression, however, was not different in SMLPL$^{-/-}$ mice. SCD-1 has also been identified along with several other genes involved in lipogenesis as a direct target of PPAR-γ in liver. Furthermore, SCD-1 plays a pivotal role in the regulation of hepatic and plasma lipoprotein TG concentrations, and SCD-1–deficient mice are usually protected against hypertriglyceridemia (34). Interestingly, SMLPL$^{-/-}$ mice had a borderline increase of plasma TG, despite the lower SCD-1 mRNA in liver. Moreover, PPAR-γ is usually associated with greater liver TG storage, and hepatic overexpression of this transcription factor leads to steatosis (35). Given that both PPAR-γ and SCD-1 mRNAs are lower and PGC-1α is higher in the livers of SMLPL$^{-/-}$ mice, the liver might respond to the excess delivery of FFAs by maintaining a higher rate of gluconeogenesis during insulin infusion in the clamp study.

To summarize and conclude, the loss of SMLPL reduced skeletal muscle TG and increased insulin sensitivity. Despite the lack of change in whole-body insulin sensitivity at a young age, insulin resistance in WAT, liver, and heart was already evident. In the skeletal muscle of young SMLPL$^{-/-}$ mice, insulin signaling at the level of Akt was increased, suggesting that LPL-derived lipids influence both basal and insulin-stimulated Akt activation. Because the reduction of LPL-dependent lipid processing in skeletal muscle must result in the partitioning of TG-rich lipoproteins to other tissues, over time this promotes

obesity development, a condition further enhanced by high-fat feeding.

ACKNOWLEDGMENTS

This work was supported by grant NIDDK-26356 (to R.H.E.) and was partially supported by grant NIHDK-059767 (to J.E.F.); CO CNRU Core Grant NIH-P30DK048520; American Diabetes Association Grant 1-04-RA-47 (to J.K.K.); the Pennsylvania State Department of Health (Tobacco Settlement Award to J.K.K.); NIH R01: DK-40936, U24: DK-76169, and P30: DK-45735; and a Distinguished Clinical Scientist Award from the American Diabetes Association (all awards to G.I.S.).

No potential conflicts of interest relevant to this article were reported.

The authors are grateful for the technical assistance from Jennifer Yoon in the laboratory of Dr. Eckel's group for ELISA assays of mouse plasma samples and mouse colony breeding and maintenance. We thank Pamila Allen at the Adult General Clinical Research Center at University of Colorado Denver for assistance with measuring mouse plasma lipids. We also thank Mario Kahn from the Department of Internal Medicine at Yale University School of Medicine for assistance in ceramide measurement.

REFERENCES

1. Merkel M, Eckel RH, Goldberg IJ: Lipoprotein lipase: genetics, lipid uptake, and regulation. *J Lipid Res* 43:1997–2006, 2002
2. Eckel RH: Lipoprotein lipase: a multifunctional enzyme relevant to common metabolic diseases. *N Engl J Med* 320:1060–1068, 1989
3. Zechner R: The tissue-specific expression of lipoprotein lipase: implications for energy and lipoprotein metabolism. *Curr Opin Lipidol* 8:77–88, 1997
4. Goldberg IJ, Merkel M: Lipoprotein lipase: physiology, biochemistry, and molecular biology. *Front Biosci* 6:D388–D405, 2001
5. Ferraro RT, Eckel RH, Larson DE, Fontvieille AM, Rising R, Jensen DR, Ravussin E: Relationship between skeletal muscle lipoprotein lipase activity and 24-hour macronutrient oxidation. *J Clin Invest* 92:441–445, 1993
6. Kim JK, Fillmore JJ, Chen Y, Yu C, Moore IK, Pypaert M, Lutz EP, Kako Y, Velez-Carrasco W, Goldberg IJ, Breslow JL, Shulman GI: Tissue-specific overexpression of lipoprotein lipase causes tissue-specific insulin resistance. *Proc Natl Acad Sci U S A* 98:7522–7527, 2001
7. Augustus A, Yagyu H, Haemmerle G, Bensadoun A, Vikramadithyan RK, Park SY, Kim JK, Zechner R, Goldberg IJ: Cardiac-specific knock-out of lipoprotein lipase alters plasma lipoprotein triglyceride metabolism and cardiac gene expression. *J Biol Chem* 279:25050–25057, 2004
8. Wredenberg A, Wibom R, Wilhelmsson H, Graff C, Wiener HH, Burden SJ, Oldfors A, Westerblad H, Larsson NG: Increased mitochondrial mass in mitochondrial myopathy mice. *Proc Natl Acad Sci U S A* 99:15066–15071, 2002
9. Eckel RH, Kern PA, Sadur CN, Yost TJ: Methods for studying lipoprotein lipase in human adipose tissue. In *Methods in Diabetes Research*. Pohl SL, Clarke WL, Larner J, Eds. New York, Wiley, 1986, p. 259–273
10. Schroeder-Gloeckler JM, Rahman SM, Janssen RC, Qiao L, Shao J, Roper M, Fischer SJ, Lowe E, Orlicky DJ, McManaman JL, Palmer C, Gitomer WL, Huang W, O'Doherty RM, Becker TC, Klemm DJ, Jensen DR, Pulawa LK, Eckel RH, Friedman JE: CCAAT/enhancer-binding protein beta deletion reduces adiposity, hepatic steatosis, and diabetes in Lepr(db/db) mice. *J Biol Chem* 282:15717–15729, 2007
11. Bligh EG, Dyer WJ: A rapid method of total lipid extraction and purification. *Can J Biochem Physiol* 37:911–917, 1959
12. Neschen S, Moore I, Regittnig W, Yu CL, Wang, Y, Pypaert M, Petersen KF, Shulman GI: Contrasting effects of fish oil and safflower oil on hepatic peroxisomal and tissue lipid content. *Am J Physiol Endocrinol Metab* 282:E395–E401, 2002
13. Choi CS, Savage DB, Abu-Elheiga L, Liu ZX, Kim S, Kulkarni A, Distefano A, Hwang YJ, Reznick RM, Codella R, Zhang D, Cline GW, Wakil SJ, Shulman GI: Continuous fat oxidation in acetyl-CoA carboxylase 2 knockout mice increases total energy expenditure, reduces fat mass, and improves insulin sensitivity. *Proc Natl Acad Sci U S A* 104:16480–16485, 2007
14. Yu C, Chen Y, Cline GW, Zhang D, Zong H, Wang Y, Bergeron R, Kim JK, Cushman SW, Cooney GJ, Atcheson B, White MF, Kraegen EW, Shulman GI: Mechanism by which fatty acids inhibit insulin activation of insulin receptor substrate-1 (IRS-1)-associated phosphatidylinositol 3-kinase activity in muscle. *J Biol Chem* 277:50230–50236, 2002
15. Jensen DR, Gayles EC, Ammon S, Phillips R, Eckel RH: A self-correcting indirect calorimeter system for the measurement of energy balance in small animals. *J Appl Physiol* 90:912–918, 2001
16. Kim HJ, Higashimori T, Park SY, Choi H, Dong J, Kim YJ, Noh HL, Cho YR, Cline G, Kim YB, Kim JK: Differential effects of interleukin-6 and -10 on skeletal muscle and liver insulin action in vivo. *Diabetes* 53:1060–1067, 2004
17. McCurdy CE, Davidson RT, Cartee GD: Brief calorie restriction increases Akt2 phosphorylation in insulin-stimulated rat skeletal muscle. *Am J Physiol Endocrinol Metab* 285:E693–E700, 2003
18. Cartee GD, Bohn EE: Growth hormone reduces glucose transport but not GLUT-1 or GLUT-4 in adult and old rats. *Am J Physiol* 268:E902–E909, 1995

18a. Vandesompele J, De Preter K, Pattyn F, Poppe B, Van Roy N, De Paepe A, Speleman F: Accurate normalization of real-time quantitative RT-PCR data by geometric averaging of multiple internal control genes. *Genome Biol* 3:RESEARCH0034, 2002

19. Sparks JD, Sparks CE: Overindulgence and metabolic syndrome: Is FoxO1 a missing link? *J Clin Invest* 118:2012–2015, 2008
20. Mora A, Komander D, van Aalten DM, Alessi DR: PDK1, the master regulator of AGC kinase signal transduction. *Semin Cell Dev Biol* 15:161–170, 2004
21. Wang XL, Zhang L, Youker K, Zhang MX, Wang J, LeMaire SA, Coselli JS, Shen YH: Free fatty acids inhibit insulin signaling-stimulated endothelial nitric oxide synthase activation through upregulating PTEN or inhibiting Akt kinase. *Diabetes* 55:2301–2310, 2006
22. Buettner R, Ottinger I, Gerhardt-Salbert C, Wrede CE, Scholmerich J, Bollheimer LC: Antisense oligonucleotides against the lipid phosphatase SHIP2 improve muscle insulin sensitivity in a dietary rat model of the metabolic syndrome. *Am J Physiol Endocrinol Metab* 292:E1871–E1878, 2007
23. Bessesen DH, Robertson AD, Eckel RH: Weight reduction increases adipose but decreases cardiac LPL in reduced-obese Zucker rats. *Am J Physiol* 261:E246–E251, 1991
24. Eckel RH, Yost TJ: Weight reduction increases adipose tissue lipoprotein lipase responsiveness in obese women. *J Clin Invest* 80:992–997, 1987
25. Eckel RH, Yost TJ, Jensen DR: Sustained weight reduction in moderately obese women results in decreased activity of skeletal muscle lipoprotein lipase. *Eur J Clin Invest* 25:396–402, 1995
26. Taskinen MR, Nikkila EA: Lipoprotein lipase of adipose tissue and skeletal muscle in human obesity: response to glucose and to semistarvation. *Metabolism* 30:810–817, 1981
27. Terrettaz J, Cusin I, Etienne J, Jeanrenaud B: In vivo regulation of adipose tissue lipoprotein lipase in normal rats made hyperinsulinemic and in hyperinsulinemic genetically-obese (fa/fa) rats. *Int J Obes Relat Metab Disord* 18:9–15, 1994
28. Hresko RC, Mueckler M: mTOR.RICTOR is the Ser473 kinase for Akt/protein kinase B in 3T3–L1 adipocytes. *J Biol Chem* 280:40406–40416, 2005
29. Bayascas JR, Alessi DR: Regulation of Akt/PKB Ser473 phosphorylation. *Mol Cell* 18:143–145, 2005
30. Maira SM, Galetic I, Brazil DP, Kaech S, Ingley E, Thelen M, Hemmings BA: Carboxyl-terminal modulator protein (CTMP), a negative regulator of PKB/Akt and v-Akt at the plasma membrane. *Science* 294:374–380, 2001
31. Qi L, Heredia JE, Altarejos JY, Screaton R, Goebel N, Niessen S, Macleod IX, Liew CW, Kulkarni RN, Bain J, Newgard C, Nelson M, Evans RM, Yates J, Montminy M: TRB3 links the E3 ubiquitin ligase COP1 to lipid metabolism. *Science* 312:1763–1766, 2006
32. Gao T, Furnari F, Newton AC: PHLPP: a phosphatase that directly dephosphorylates Akt, promotes apoptosis, and suppresses tumor growth. *Mol Cell* 18:13–24, 2005
33. Darimont C, Avanti O, Zbinden I, Leone-Vautravers P, Mansourian R, Giusti V, Mace K: Liver X receptor preferentially activates de novo lipogenesis in human preadipocytes. *Biochimie* 88:309–318, 2006
34. Flowers JB, Rabaglia ME, Schueler KL, Flowers MT, Lan H, Keller MP, Ntambi JM, Attie AD: Loss of stearoyl-CoA desaturase-1 improves insulin sensitivity in lean mice but worsens diabetes in leptin-deficient obese mice. *Diabetes* 56:1228–1239, 2007
35. Yu S, Viswakarma N, Batra SK, Sambasiva RM, Reddy JK: Identification of promethin and PGLP as two novel up-regulated genes in PPARgamma1-induced adipogenic mouse liver. *Biochimie* 86:743–761, 2004